Multidisciplinary Journal of Horseed International University (MJHIU)
ISSN 2959-4154
Vol. 3, Issue 2, 2025
DOI: http://dx.doi.org/10.59336/h3t6bd65

RESEARCH ARTICLE

Ameliorative Effects of Ginger-Zinc Oxide Nanoparticles on Lead Nitrate-Induced Oxidative Stress in Wistar Rats

John Moyinoluwa Ajayi[1,2*], Juliana Bunmi Adetunji[1] and Olu Israel Oyewole[1]

[1]*Department of Biochemistry, Osun State University, Osogbo, Nigeria;* [2]*Department of Biochemistry, Adeleke University, Ede, Osun State, Nigeria*

Received: August 25, 2025
Accepted: September 01, 2025
Published: September 25, 2025

Abstract: Lead exposure disrupts male reproductive health, however, natural antioxidants and trace elements may offer protection against such effects. This study investigated the protective efficacy of ginger-zinc oxide nanoparticles (G-ZO Nps) against lead nitrate-induced testicular toxicity in Wistar rats.

Zinc oxide nanoparticles were synthesized and characterized by Ultraviolet-Visible (UV-VIS) spectroscopy, Fourier Transformed Infrared Spectroscopy (FTIR), Scanning Electron Microscopy-Energy Dispersive X-ray Spectroscopy (SEM-EDX), and High-Performance Liquid Chromatography (HPLC). Twenty rats were divided into five groups: control, lead nitrate, ginger extract, G-ZO Nps, and zinc acetate. Treatments lasted 28 days *via* oral gavage, after which testicular tissues were subjected to biochemical, and histological analyses. Moreover, *in silico* molecular docking was conducted on twelve G-ZO Nps derived flavonoids and zinc acetate against three reproductive proteins using AutoDock Vina, with ligand-protein interactions visualized *via* Discovery Studio Visualizer. SwissADME was also employed to assess pharmacokinetic and drug-likeness profiles.

Lead nitrate markedly suppressed superoxide dismutase (SOD) and catalase (CAT) activities, slightly elevated glutathione peroxidase (GPx) and glutathione (GSH) levels, demonstrated no effect on malondialdehyde (MDA) levels, significantly increased nitric oxide (NO) levels, and caused degeneration of seminiferous tubules. G-ZO Nps restored antioxidant balance and preserved testicular histoarchitecture more effectively than ginger extract or zinc acetate. Molecular docking identified apigenin, isoquercetin, and myricetin 3-O-galactoside as the most stable flavonoids (–9.8 to –9.9 kcal/mol), with superior drug-likeness and bioavailability confirmed by SwissADME, while zinc acetate showed weak binding.

It can be concluded that G-ZO Nps demonstrated potent antioxidative and histoprotective effects against lead-induced testicular injury, surpassing both ginger extract and zinc acetate. These findings position *Z. officinale* nanoparticles as a promising nanotherapeutic strategy for mitigating heavy metal–induced reproductive toxicity.

Keywords: Nanomedicine, antioxidants, lead toxicity, oxidative stress, and testicular damage.

1. INTRODUCTION

Lead (Pb) is a pervasive environmental contaminant that causes multisystem toxicity, with the male reproductive system being particularly vulnerable. Chronic Pb exposure disrupts spermatogenesis and tes-

**Correspondence should be addressed to John Moyinoluwa Ajayi, Department of Biochemistry, Osun State University, Osogbo, Nigeria; Department of Biochemistry, Adeleke University, Ede, Osun State, Nigeria; E-mail: ajayi.john@adelekeuniversity.edu.ng*

ticular function through oxidative stress, lipid peroxidation, and impaired antioxidant enzyme activity (Kumar, 2020; Zheng *et al.,* 2023). These effects are mediated by overproduction of reactive oxygen and nitrogen species, which overwhelm endogenous defense systems and trigger testicular degeneration (Tuncer *et al.,* 2023).

Natural antioxidants have gained attention as protective agents against heavy-metal–induced oxidative injury. *Zingiber officinale* (ginger) is a medicinal plant rich in phenolic compounds and flavonoids such as gingerols and shogaols (Unuofin *et al.,* 2021), which possess radical-scavenging, anti-inflammatory, and cytoprotective activities (Gholami-Ahangaran *et al.,* 2021; Saha *et al.,* 2018; El-Ashmawy *et al.,* 2018). Recent evidence shows that ginger supplementation enhances antioxidant enzyme activities and mitigates reproductive toxicity in experimental models (Abdelfattah *et al.,* 2023; Funmilola *et al.,* 2025).

However, the therapeutic efficiency of plant-derived antioxidants is often limited by poor solubility and bioavailability. Nanotechnology provides a strategy to overcome these limitations by improving delivery, stability, and cellular uptake of bioactive compounds (Mutukwa *et al.,* 2024). Zinc oxide nanoparticles (ZnO Nps) are particularly attractive due to their low cost, large surface area, and favorable biomedical properties. Plant-mediated "green synthesis" of ZnO Nps using phytochemicals as reducing and stabilizing agents yields eco-friendly, bioactive nanoparticles suitable for therapeutic use (Al-Darwesh *et al.,* 2024; Jaishi *et al.,* 2024).

While studies have described the preparation of ZnO Nps using *Z. officinale* extracts (Al-Suwayyid *et al.,* 2023; Alhaddad *et al.,* 2024), translational investigations applying such formulations specifically to male reproductive protection remain sparse. Although, several studies have evaluated the separate reproprotective roles of zinc and zinc oxide nanoparticles, however, there is little systematic evidence evaluating the combined protective effect of ginger–ZnO nanoparticles (G-ZO Nps) specifically against Pb-induced testicular toxicity (Maher *et al.,* 2024; Besong *et al.,* 2023). Furthermore, there is paucity of information regarding direct comparison between the efficacy of ginger-derived zinc oxide nanoparticles, crude ginger extract and zinc salts in reproductive toxicity models. These gaps justify an integrated evaluation of synthesis, *in vivo* antioxidative efficacy, histomorphological outcomes, and complementary in silico analyses of ginger-derived flavonoid interactions with reproductive protein targets.

1.1. Hypothesis and Objective

We hypothesize that G-ZO Nps will provide superior protection against Pb-induced testicular toxicity compared to crude ginger extract or zinc acetate, by enhancing antioxidant defenses and preserving testicular histoarchitecture. This study therefore aimed to synthesize and characterize G-ZO Nps, evaluate their *in vivo* efficacy in lead nitrate exposed male Wistar rats, and complement these findings with in silico docking of G-ZO Nps derived flavonoids against key reproductive proteins.

2. METHODOLOGY

2.2. Preparation of Ginger Extract and Green Synthesis of Ginger-Zinc Oxide Nanoparticles

2.2.1. Preparation of Hydroethanolic Ginger Extract

Fresh rhizomes of *Zingiber officinale* (ginger) were purchased from a local market Osogbo, Osun State Nigeria. The rhizomes were thoroughly washed with distilled water, sliced into thin pieces, and air-dried under shade at room temperature (25–28 °C) for 10 days to preserve bioactive constituents. The dried ginger was ground into a fine powder and stored in airtight containers. A 40% hydroethanolic solution was used as the extraction solvent. This choice of this solvent was to optimize the recovery of both polar and moderately non-polar bioactive compounds from ginger. Ethanol-water mixtures are widely recognized for their efficiency in extracting a broad spectrum of phytochemicals including flavonoids and phenolics which were of specific interest in this study, which may not be effectively extracted using either pure water or pure ethanol alone. Moreover, hydroethanolic mixtures are safe, environmentally friendly, and compatible with downstream biological applications, making them a preferred solvent system in pharmacological and nutraceutical research.

About 100 g of ginger powder was macerated in 1 L of 40% ethanol for 24 hours with occasional shaking. The mixture was filtered through Whatman No. 1 filter paper, and the filtrate was concentrated through evaporation by heating in a water bath at 40^0 C. The concentrated extract was stored in airtight containers at room temperature until further use.

2.2.2. Green Synthesis of Ginger-Zinc Oxide Nanoparticles (G-ZO NPs)

Green synthesis of 0.1M ginger-zinc oxide nanoparticles was carried out using the hydroethanolic ginger extract as both the reducing and stabilizing agents, while zinc acetate dihydrate [$Zn(CH_3COO)_2 \cdot 2H_2O$] was used as the zinc precursor. Initially, 0.1 M zinc acetate solution was synthesized by dissolving 21.95g of zinc acetate dihydrate in 1L of distilled water and stirred continuously until complete dissolution. The ginger extract was then added dropwise to the 0.1M zinc acetate solution under constant stirring. The reaction mixture was maintained at 40 °C for 2 hours, during which a gradual change in color from dark brown to a pale yellow was observed, indicating the formation of zinc oxide nanoparticles. The mixture was allowed to stand for 24 hours at room temperature for complete nucleation. The synthesized nanoparticles was freeze dried and stored in an airtight container (Trenkenschuh and Friess, 2021). No external chemical reducing or capping agents were used, thus conforming to eco-friendly green synthesis principles.

2.3. Experimental Design

2.3.1. Animals and Housing

Twenty (20) male Wistar rats weighing between 80 and 125 grams were used in this study. The animals were obtained from a certified breeding facility and housed in standard polypropylene cages under controlled environmental conditions: temperature (22 ± 2 °C), relative humidity (50–60%), and a 12-hour light/dark cycle. All animals were acclimatized for one week prior to the start of the experiment and had unrestricted access to pelletized rat chow and clean water *ad libitum*.

2.3.2. Ethical Approval

All procedures involving animals were conducted in accordance with internationally accepted guidelines for the care and use of laboratory animals. Ethical approval for the study was obtained from the Adeleke University Ethics Committee (AUEC), under approval number **AUERC/2025/66BCH/01**.

2.3.3. Animal Grouping and Treatment

After acclimatization, the animals were randomly assigned into five experimental groups and treated once daily *via* oral gavage for 28 consecutive days. The treatment regimens were as follows:

Control: Received distilled water only.

$(PbNO_3)_2$: Received 100 mg/kg body weight of lead nitrate.

$(PbNO_3)_2$ + Z.O Nps: Received 100 mg/kg of lead nitrate and 100 mg/kg of ginger oxide nanoparticles.

$(PbNO_3)_2$ + Z.O Extract: Received 100 mg/kg of lead nitrate and 100 mg/kg of hydroethanolic ginger extract.

$(PbNO_3)_2$ + Zinc Acetate: Received 100 mg/kg of lead nitrate and 100 mg/kg of zinc acetate.

All substances were administered orally in a volume of 1 ml per 100 g body weight using an intragastric gavage needle.

2.3.4. Biochemical Assays

After the 28 days treatment period, rats were euthanized *via* cervical dislocation using ketamine as the anesthesia. The testes were quickly excised, rinsed in ice-cold normal saline, blotted dry, and homogenized in phosphate buffer (0.1 M, pH 7.4) using a glass homogenizer. The homogenates were centrifuged at 10,000 rpm for 15 minutes at 4 °C. The supernatants were collected and stored at −20 °C until further

biochemical analysis. The following oxidative stress markers and antioxidant enzyme activities were evaluated:

2.3.5. Superoxide Dismutase (SOD) Activity

SOD activity was measured according to the method described by Misra and Fridovich (1972). This method is based on the ability of SOD to inhibit the autoxidation of epinephrine at alkaline pH (pH 10.2). The change in absorbance was read at 480 nm for 5 minutes at 1-minute intervals. One unit of SOD activity is defined as the amount of enzyme required to cause 50% inhibition of epinephrine autoxidation.

2.3.6. Catalase (CAT) Activity

CAT activity was determined using the method of Aebi (1984). This assay measures the decomposition of hydrogen peroxide (H_2O_2) by catalase in the testis homogenates. The reduction in absorbance was recorded at 240 nm over a period of 1 minute.

2.3.7. Glutathione Peroxidase (GPx) Activity

GPx activity was measured using the method described by Rotruck et al. (1973). This assay evaluates the enzyme's ability to reduce hydrogen peroxide by oxidizing reduced glutathione (GSH), with the residual GSH measured by its reaction with 5,5'-dithiobis-2-nitrobenzoic acid (DTNB) at an absorbance of 412nm.

2.3.8. Reduced Glutathione (GSH) Concentration

GSH levels were quantified using the Ellman method (1959). This method involves the reduction of DTNB (Ellman's reagent) by free thiol groups in GSH to form a yellow-colored 5-thio-2-nitrobenzoic acid (TNB), which is read spectrophotometrically at an absorbance of 412nm.

2.3.9. Nitric Oxide (NO) Level

NO levels were estimated indirectly by measuring nitrite (a metabolite of NO) accumulation in tissue homogenates using the Griess reaction, according to the method described by Grisham et al. (1996) and modified by Guevara et al. (1998). Sulfanilamide and N-(1-naphthyl)ethylenediamine react with nitrite in acidic medium to form a diazonium compound, which is then measured colorimetrically at an absorbance of 540nm.

2.3.10. Malondialdehyde (MDA) Level

MDA, a by-product of lipid peroxidation, was determined using the Thiobarbituric Acid Reactive Substances (TBARS) method. MDA reacts with thiobarbituric acid (TBA) under acidic and high-temperature conditions to form a pink chromogen which is then measured spectrophotometrically at an absorbance of 532 nm.

2.4. Histological Procedures

After euthanasia, the testes were excised and immediately fixed in 10% neutral-buffered formalin for 48 hours. The fixed tissues were then dehydrated through a graded series of ethanol, cleared in xylene, and embedded in paraffin wax. Tissue sections of 5 µm thickness were cut using a rotary microtome and mounted on glass slides. The sections were deparaffinized, rehydrated, and stained with hematoxylin and eosin (H&E) for general histological examination.

The stained slides were examined under a light microscope (×40 magnification), and photomicrographs were taken using a digital photomicroscope. Structural integrity of seminiferous tubules, spermatogenic activity, Leydig cell presence, and signs of pathological changes such as vacuolation, epithelial disorganization, or necrosis were assessed.

2.5. Statistical Analysis

All data were presented as mean ± standard error of mean (SEM). Statistical comparisons between groups were performed using one-way analysis of variance (ANOVA) followed by Tukey's multiple

comparisons test using GraphPad Prism version 10.2.0. A p-value < 0.05 was considered statistically significant.

2.6. In Silico Analysis and Molecular Docking

The three-dimensional (3D) structures of the androgen receptor (PDB ID: 1T7R), PDE-5 (PDB ID: 3HDZ), and the human SRY protein (PDB ID: 1J46) were retrieved from the Protein Data Bank (PDB). Ligands, including zinc acetate and phytochemicals identified from G-O nanoparticles, were obtained from the PubChem database. Ligand preparation and energy minimization were performed in PyRx and converted to PDBQT format, while receptor proteins were prepared using AutoDock Vina by removing water molecules, adding polar hydrogens, and assigning Gasteiger charges. Docking simulations were conducted using PyRx, with grid boxes centered on the binding sites. Docking scores were recorded in kcal/mol, and the top-ranked conformations were analyzed. Pharmacokinetics and drug-likeness properties, including Lipinski's rule of five, bioavailability, lipophilicity, and solubility, were evaluated using the SwissADME web server. The ligand-protein binding interactions, including hydrogen bonding, hydrophobic interactions, and pi-pi stacking, were visualized using Discovery Studio Visualizer.

3. RESULTS

3.1. Nanoparticles Characterization Results

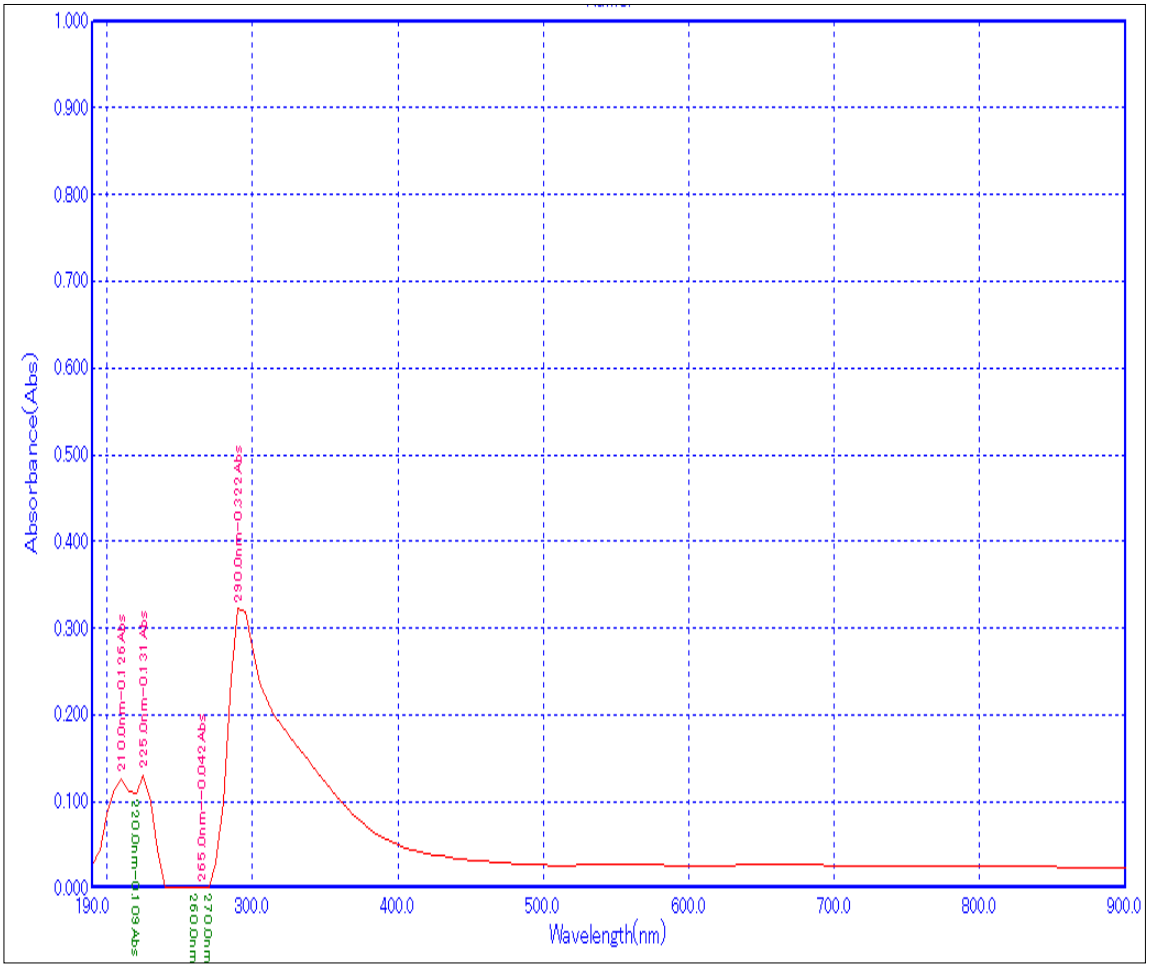

Figure 1. Graph of UV/VIS spectroscopy of G-ZO Nps.

The graph indicates an absorption maximum at a wavelength of 290nm for the synthesized nanoparticle.

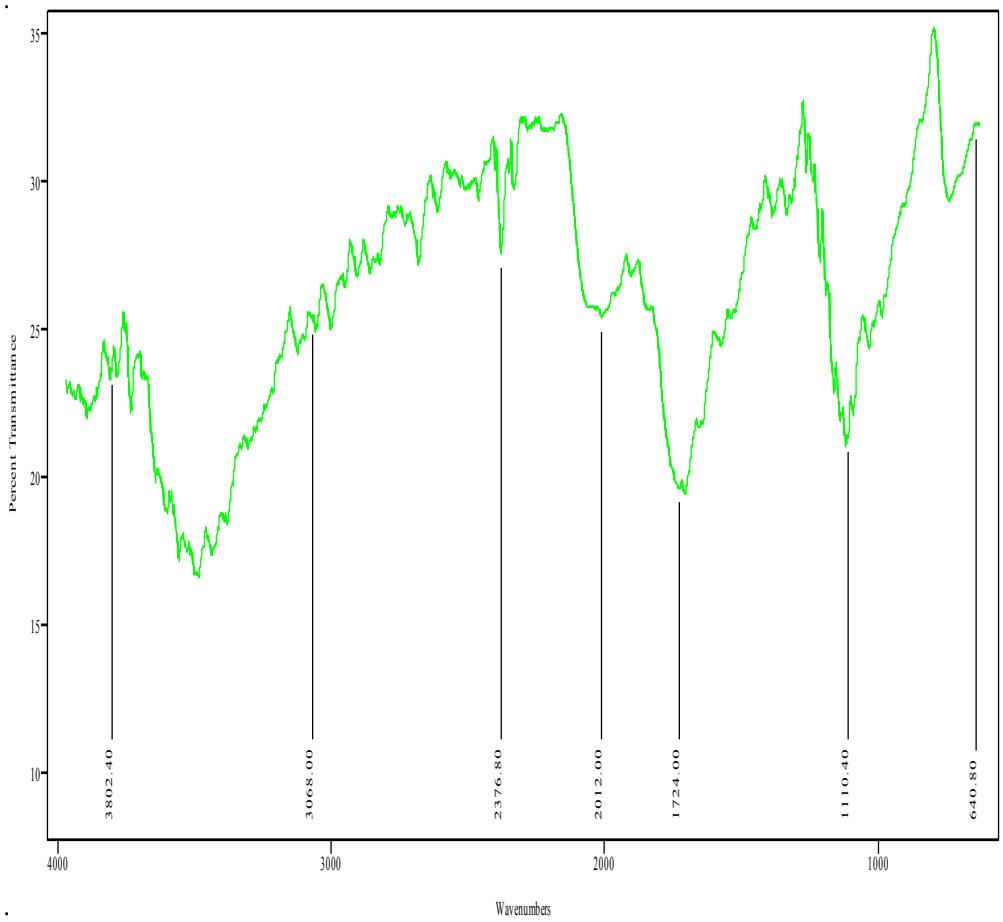

Figure 2. Graph of Fourier Transformed Infrared (FTIR) spectroscopy of G-ZO Nanoparticles.

The FTIR spectrum shows characteristic flavonoid functional groups, including C=O (1724 cm^{-1}), C–O (1110 cm^{-1}), and aromatic C–H (3068 cm^{-1}) stretching vibrations. The Zn–O stretching vibration is observed at 640 cm^{-1}, confirming the formation of ZnO nanoparticles. Broadening of the O–H band (~3802 cm^{-1}) indicates interaction of flavonoid hydroxyl groups with the nanoparticle surface, suggesting successful capping/stabilization.

Table 1. HPLC result of flavonoids in G-ZO Nps extracts

Peak	RT (min)	Compound Detected	Peak Area %	Comp % wt
1	1.00	Phloroglucinol	5.18	5.08
2	2.13	Naringenin	10.64	10.57
3	3.20	Apigenin	18.34	18.11
4	12.00	Luteolin	3.51	3.44
5	16.00	Kaempferol	6.93	6.80
6	20.18	Quercetin	23.43	23.11
7	22.07	Myricetin-3-galactoside	4.02	3.93
8	23.50	Myricetin	8.43	8.36
9	24.86	Curcumin	4.85	4.75
10	28.00	Quercetin-3-glucoside	4.33	5.66
11	34.50	Hesperidin	7.67	7.55
12	43.19	Rutin	2.67	2.63

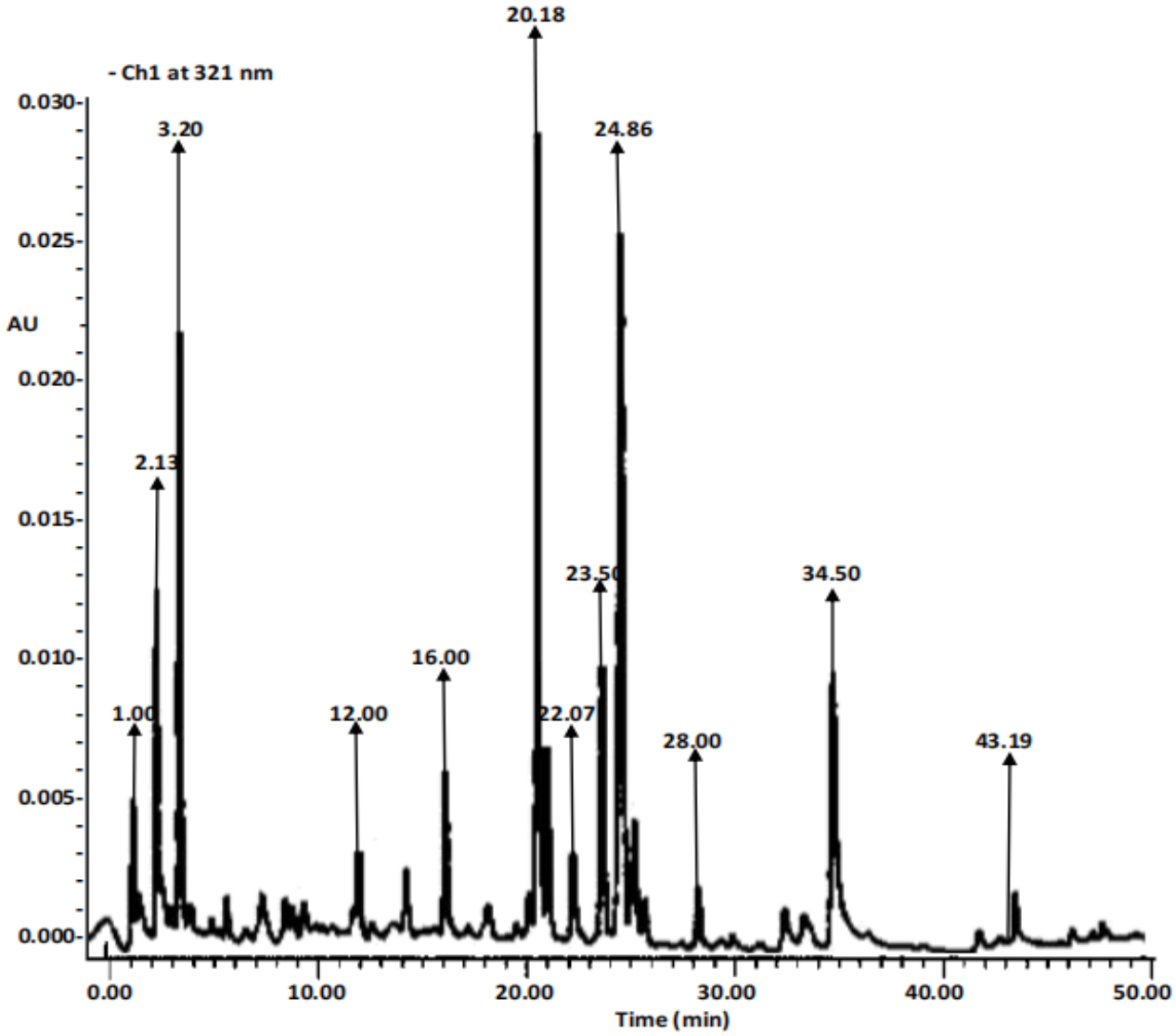

Figure 3. HPLC chromatogram of G-ZO Nps.

Table 2. SEM-EDX result of the G-ZO Nps.

Element	Composition (%)
Carbon (C)	54.93
Oxygen (O)	31.19
Zinc (Zn)	3.59
Nitrogen(N)	1.32
Sulphur(S)	0.86
Phosphorus (P)	0.45
Magnesium (Mg)	1.03
Potassium (K)	1.16
Calcium (Ca)	4.77
Copper (Cu)	0.21
Iron (Fe)	0.48

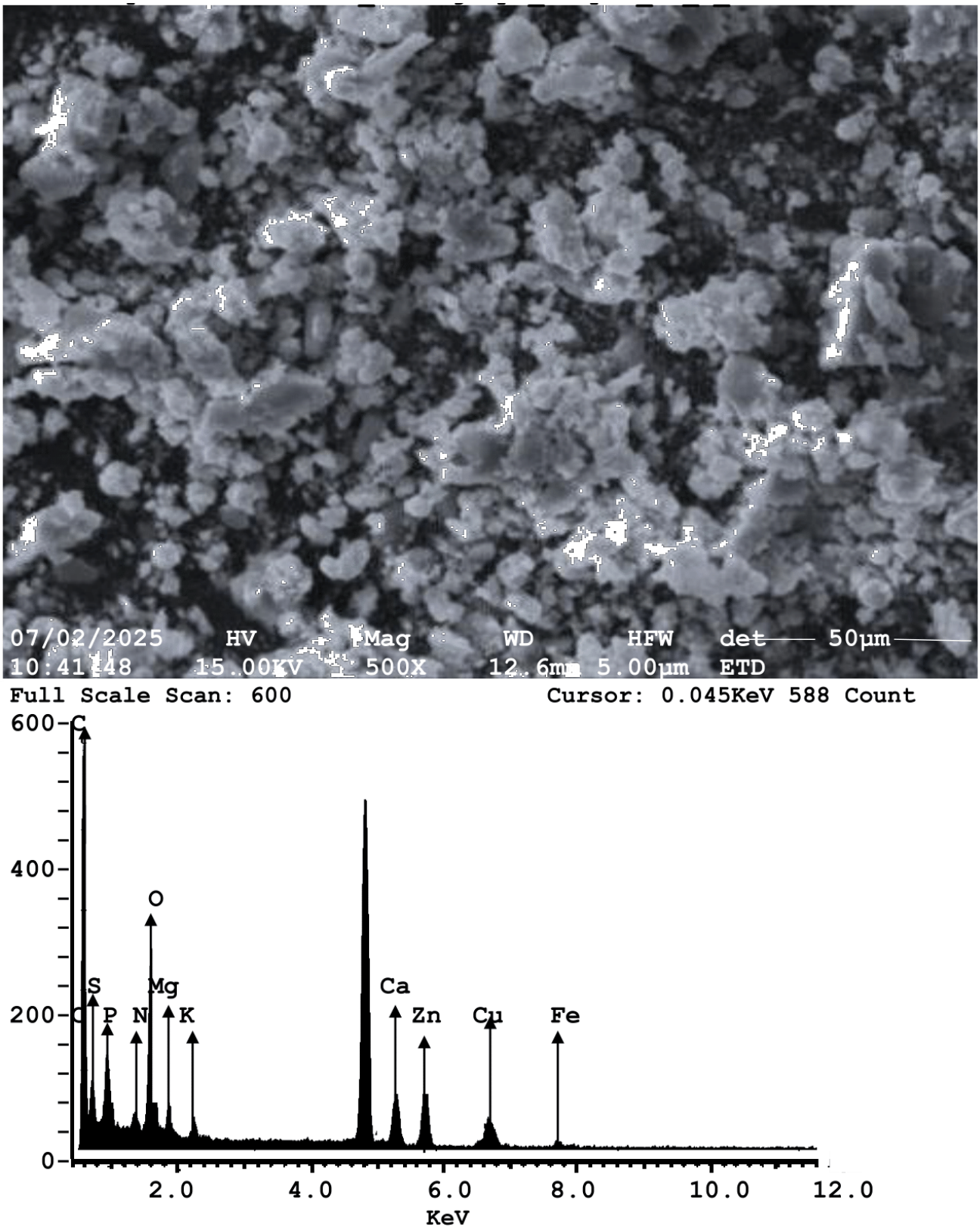

Figure 4. Scanning Electron Micrograph of G-ZO Nps (×500 magnification). Image shows a porous and spherical hexagonal that were irregular in size and shape. It has a particle size of 21.64 nm, height of 1.81 mm, and bulk density of 0.43g/cm^3.

4. RESULTS OF BIOCHEMICAL ASSAYS

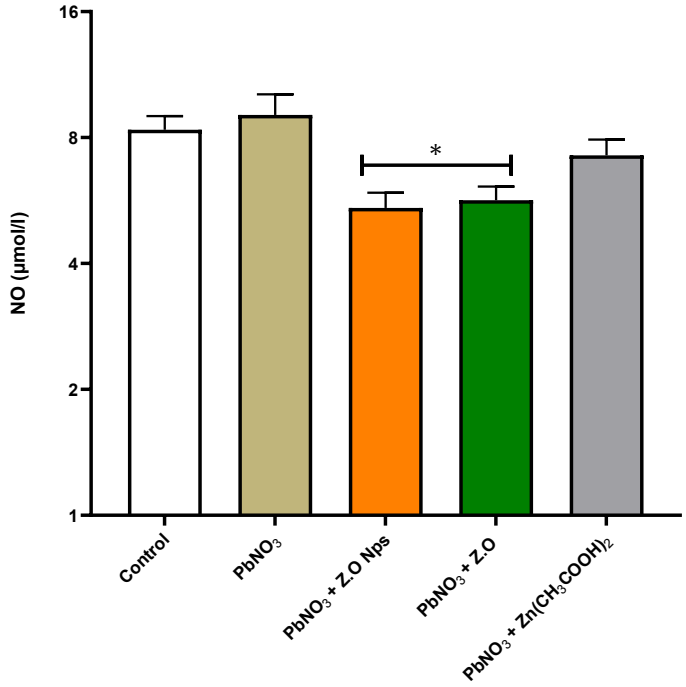

Figure 5. Effects of $Pb(NO_3)_2$ exposure and treatments on Nitric oxide (NO).

Data were expressed as Mean ± SEM (n=5). * represents $p < 0.05$ vs $Pb(NO_3)_2$ (Tukey's multiple comparisons test).

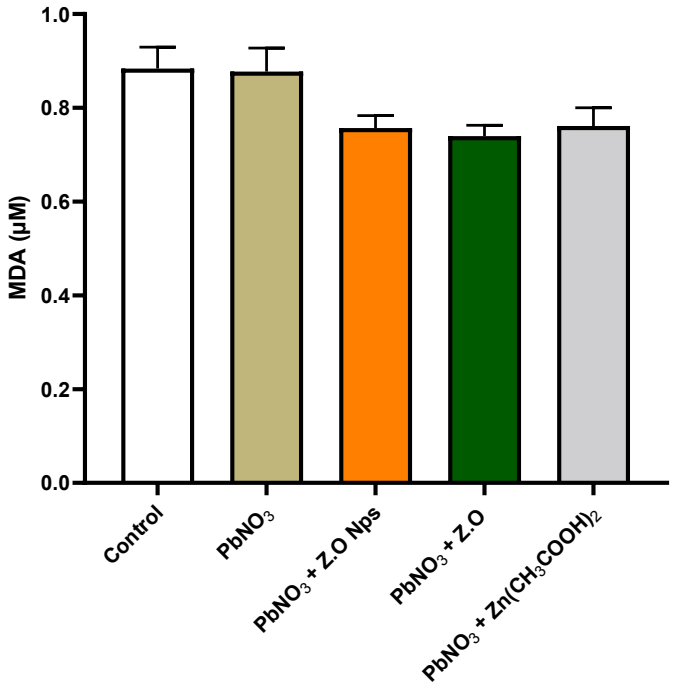

Figure 6. Effects of $Pb(NO_3)_2$ exposure and treatments on Malondialdehyde (MDA).

Data were expressed as Mean ± SEM (n=5). There was no significant difference across the groups at $p<0.05$.

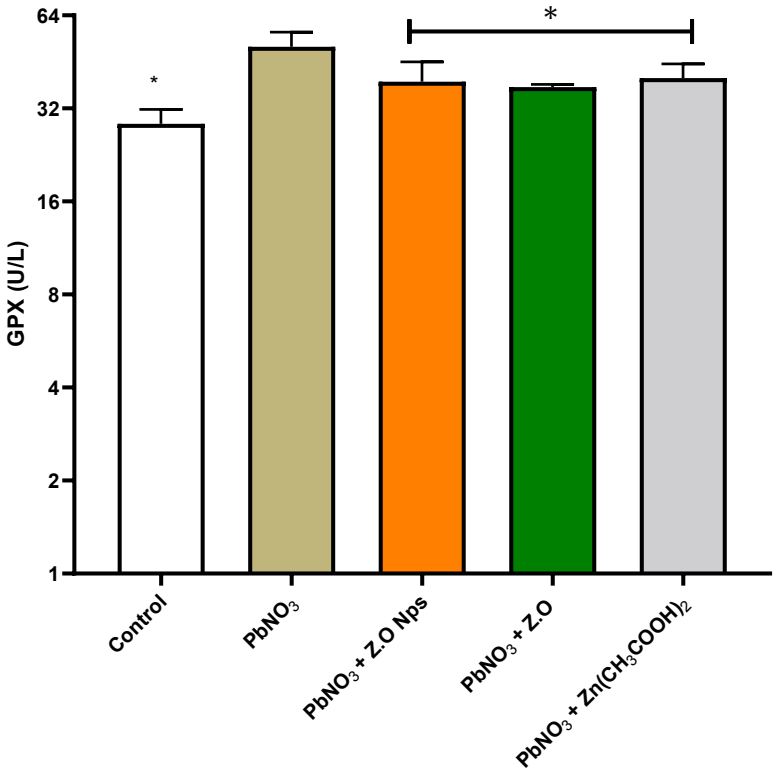

Figure 7: Effects of $Pb(NO_3)_2$ exposure and treatments on glutathione peroxidase (GPX).

Data were expressed as Mean ± SEM (n=5). Values were considered significant at $p<0.05$ using ANOVA. * represents $p < 0.05$ vs $Pb(NO_3)_2$ (Tukey's multiple comparisons test).

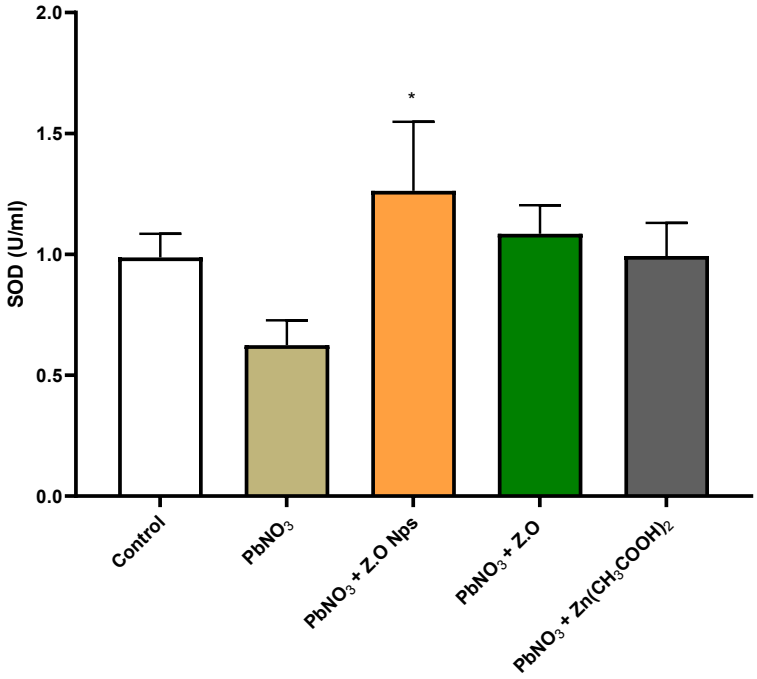

Figure 8. Effects of $Pb(NO_3)_2$ exposure and treatments on Superoxide dismutase (SOD).

Data were expressed as Mean ± SEM (n=5). * represents $p < 0.05$ vs $Pb(NO_3)_2$ (Tukey's multiple comparisons test).

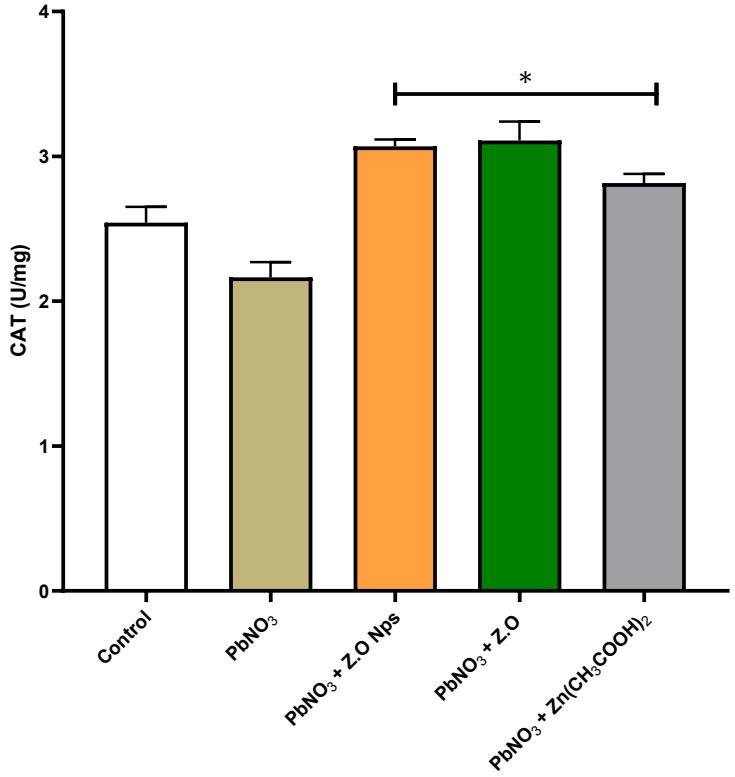

Figure 9. Effects of $Pb(NO_3)_2$ exposure and treatments on Catalase.

Data were expressed as Mean ± SEM (n=5). * represents $p < 0.05$ vs $Pb(NO_3)_2$ (Tukey's multiple comparisons test).

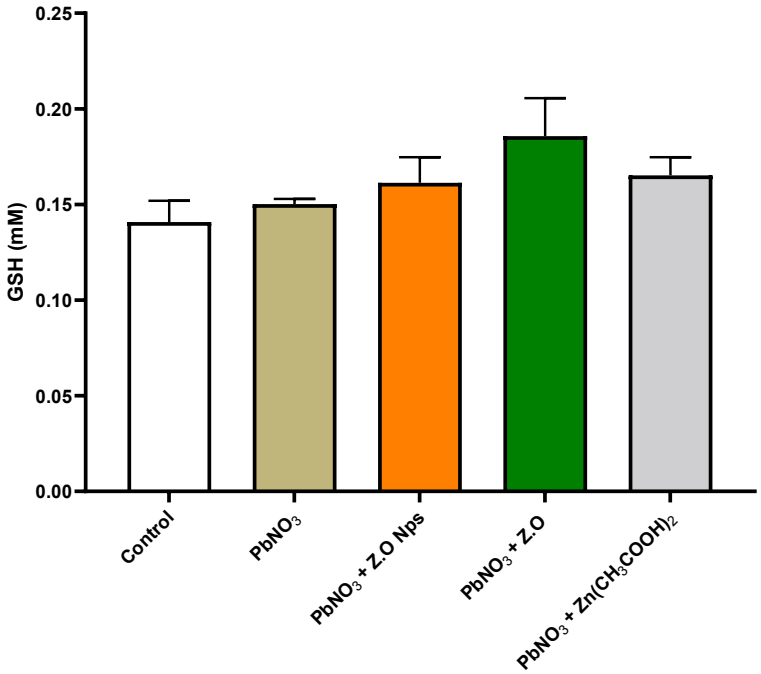

Figure 10. Effects of $Pb(NO_3)_2$ exposure and treatments on glutathione (GSH).

Data were expressed as Mean ± SEM (n=5). There was no significant differences across the groups at $p<0.05$.

4.1. Histology Results

Histological examination of hematoxylin and eosin (H&E)–stained sections of rat testes (×40 magnification) revealed distinct group-specific changes (Figure 11 a-e) which represent the photomicrographs of testes belonging to Groups 1-5 animals respectively.

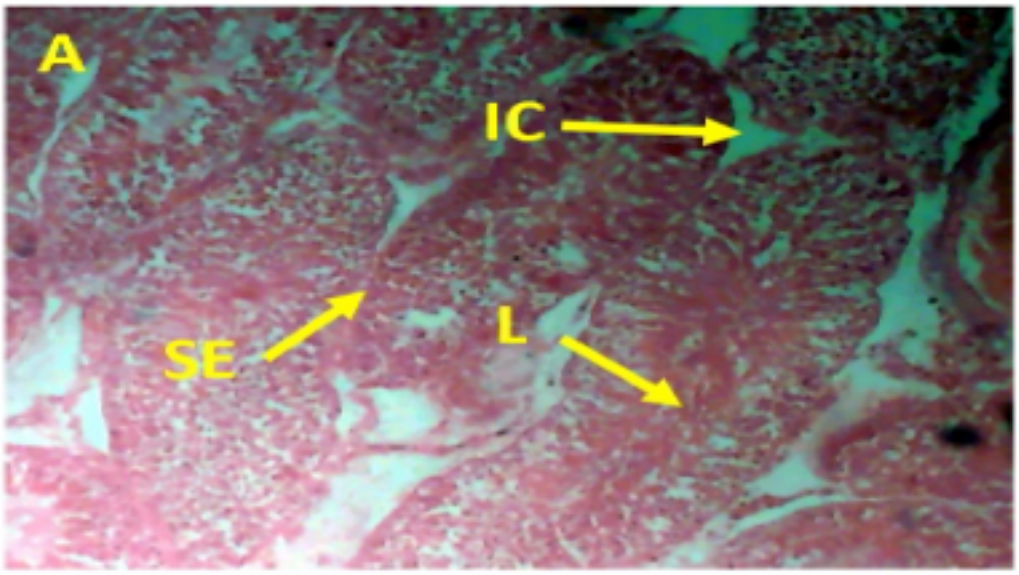

Figure 11a. Histology photomicrograph A.

It represents the photomicrographs of testes belonging to animals in the control group. Seminiferous tubules were rounded and well-defined, exhibiting dense and multilayered seminiferous epithelium (SE), with clearly delineated lumens (L) and numerous interstitial cells (IC) occupying the intertubular spaces, indicating optimal spermatogenic activity. Similarly,

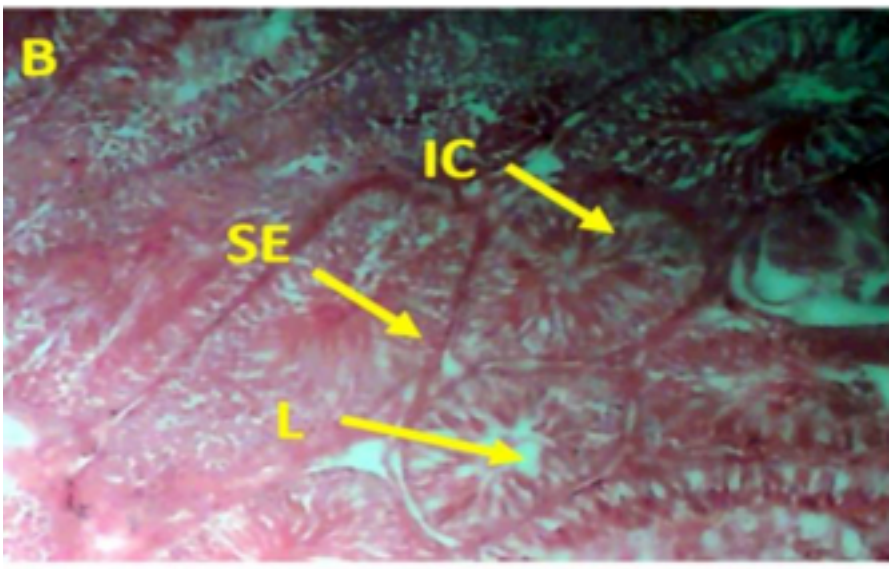

Figure 11b. Histology photomicrograph B.

It represents the photomicrographs of testes belonging to animals in the **$(PbNO_3)_2$** group.

It displayed thick seminiferous epithelium with active luminal spermatid release and prominent Leydig cell clusters, although luminal spermatozoa density was slightly diminished

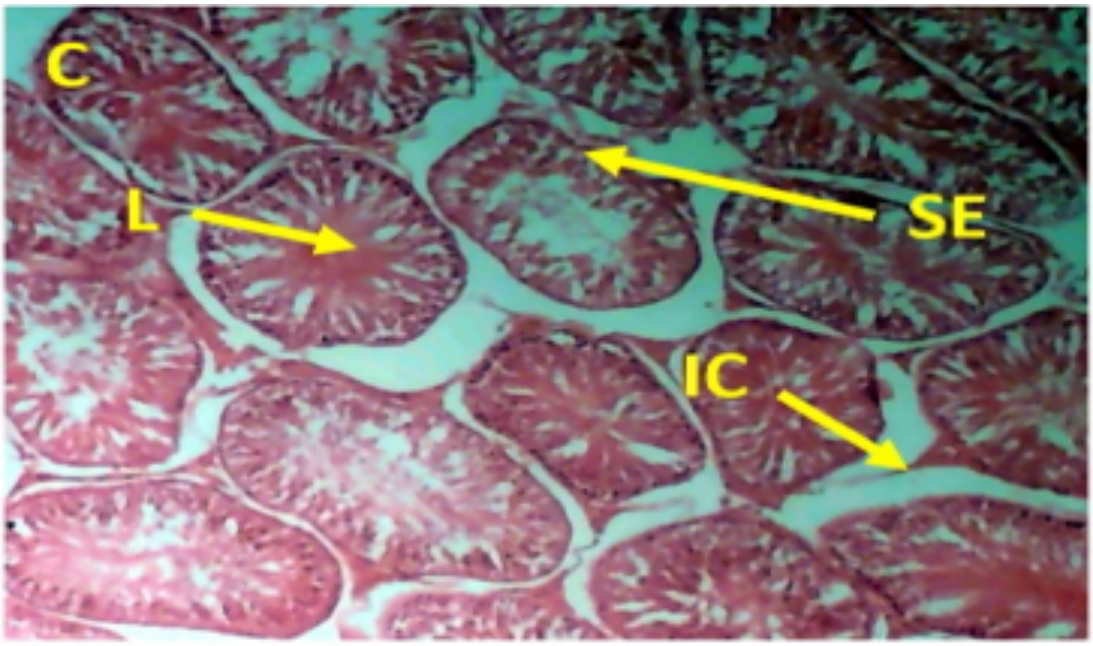

Figure 11c. Histology photomicrograph C.

It represents the photomicrographs of testes belonging to animals in the **$(PbNO_3)_2$ + Z.O Nps** group. It showed tubules with expanded lumens and slightly hypertrophied interstitial cells; although the epithelial stratification remained evident.

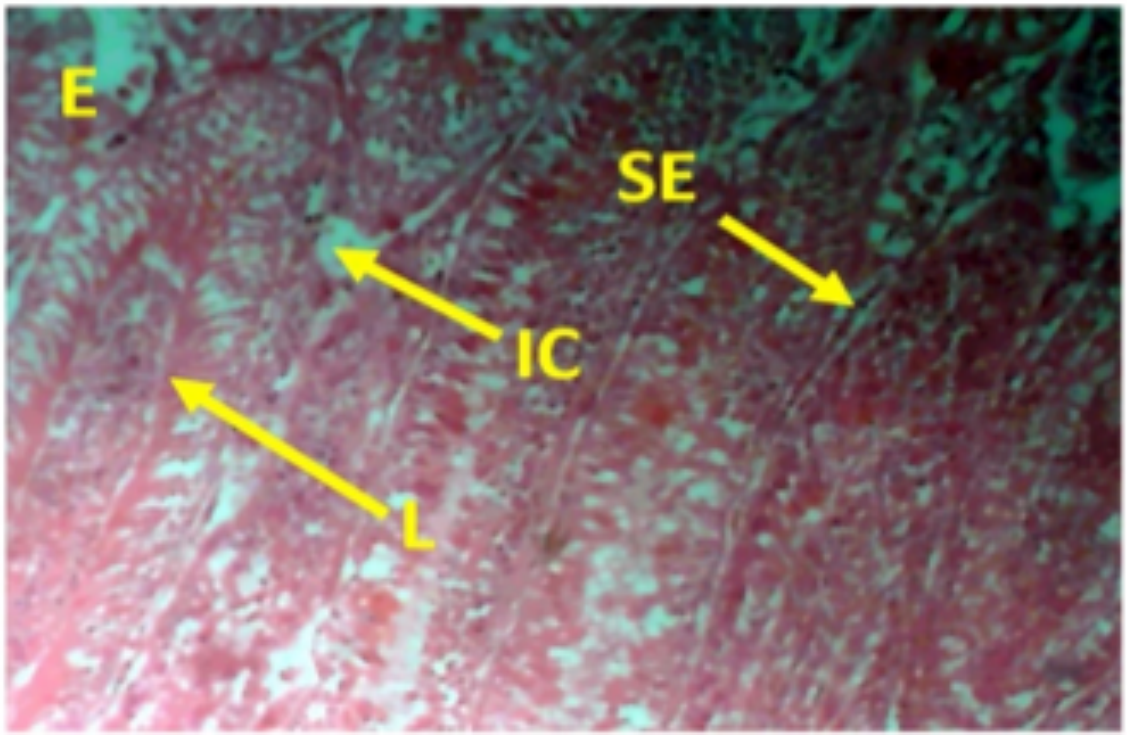

Figure 11d. Histology photomicrograph E.

It represents the photomicrographs of testes belonging to animals in the **$(PbNO_3)_2$ + Z.O** Longitudinally sectioned tubules showed attenuated epithelial height and elongated luminal profiles, with fewer visible interstitial cells.

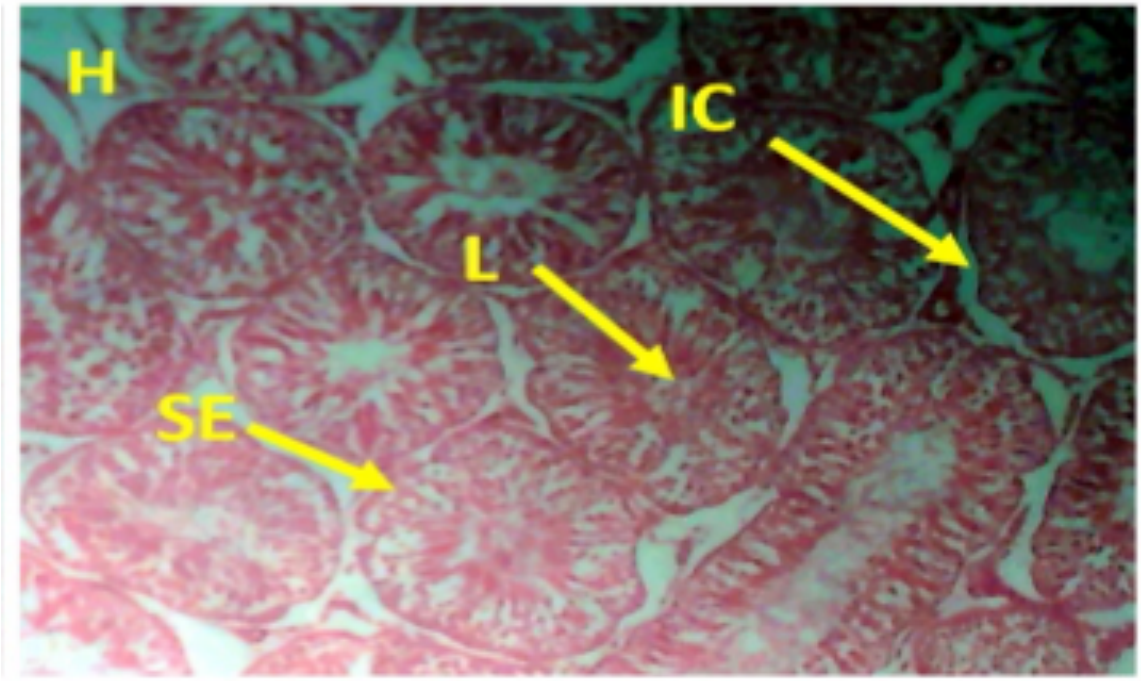

Figure 11e. Histology photomicrograph H.

It represents the photomicrographs of testes belonging to animals in the **$(PbNO_3)_2$ + Z.O**

Signs of mild epithelial vacuolation and sparse luminal content, alongside a slight reduction in Leydig cell density were observed.

Overall, no section revealed evidence of necrosis, inflammation, hemorrhage, or fibrosis, suggesting that observed changes were primarily functional or adaptive rather than overtly pathological.

4.2. *In silico* Results and Molecular Docking

Table 3. G-ZO Nps with 1j46.

Ligand	Binding Affinity (kcal/mol)
Rutin	-7.5
Hesperidin	-7.0
Curcumin	-6.9
Isoquercetin	-6.9
Myricetin 3-O-galactoside	-6.7
Luteolin	-6.7
Myricetin	-6.6
Apigenin	-6.6
Kaempferol	-6.5
Quercetin	-6.4
Naringenin	-6.3
Phloroglucinol	-4.4
Zinc acetate	-1.0

Table 4. G-ZO Nps with 1t7r.

Ligand	Binding Affinity (kcal/mol)
Rutin	-9.0
Quercetin	-8.1
Apigenin	-8.1
Myricetin	-8.1
Isoquercetin	-8.0
Hesperidin	-7.9
Naringenin	-7.9
Luteolin	-7.8
Myricetin 3-O-galactoside	-7.7
Kaempferol	-7.6
Curcumin	-7.0
Phloroglucinol	-5.0
Zinc acetate	-1.3

Table 5. G-ZO Nps with 3hdz.

Ligand	Binding Affinity (kcal/mol)
Hesperidin	-12.2
Rutin	-11.5
Myricetin 3-O-galactoside	-9.9
Apigenin	-9.8
Luteolin	-9.8
Isoquercetin	-9.8
Quercetin	-9.7
Kaempferol	-9.7
Myricetin	-9.4
Naringenin	-9.3
Curcumin	-8.7
Phloroglucinol	-5.9
Zinc acetate	-1.3

Table 6. Physicochemical properties of G-ZO Nps ligands and zinc acetate defined with the SwissADME database.

COMPOUNDS	Rutin	Isoquercetin	Apigenin	Myricetin 3-O-galactoside	Zinc acetate
Molecular formula	$C_{28}H_{34}O_{15}$	$C_{21}H_{20}O_{12}$	$C_{15}H_{10}O_5$	$C_{21}H_{20}O_{13}$	$C_4H_6O_4Zn$
Molecular weight (g/mol)	610.56	464.38	270.24	480.38	183.47
Number of heavy atoms	43	33	20	34	9
Number of aromatic heavy atoms	12	16	16	16	0
Fraction Csp3	0.54	0.29	0.00	0.29	0.50
Number of rotatable bonds	7	4	1	4	0
Number of H bond acceptor	15	12	5	13	4
Number of H bond donors	8	18	3	9	0
Molar refractivity	141.4	110.16	73.99	112.18	23.11
Topological polar surface area (TPSA)	234.29 Å²	210.51 Å²	90.90 Å	230.74 Å	80.26 Å²

Table 7. Lipophilicity and water solubility of G-ZO Nps ligands and zinc acetate calculated using the Swiss ADME database.

Compound	Lipophilicity	Water solubility					
	Consensus log $P_{o/w}$	Log S (ESOL)	Solubility Class	Log S (all)	Solubility Class	Log S (silicos-it)	Solubility Class
Rutin	-1.06	-3.28	Soluble	-4.33	Moderately soluble	-0.58	Soluble
Isoquercetin	-0.48	-3.04	Soluble	-4.35	Moderately soluble	-151	Soluble
Apigenin	2.11	-3.94	Soluble	-4.59	Moderately soluble	-4.40	Moderately soluble
Myricetin 3-O-galactoside	-0.89	-2.91	Soluble	-4.41	Moderately soluble	-0.92	Soluble
Zinc acetate	-7.67	-0.71	Very soluble	-0.8	Very soluble	0.53	Soluble

Table 8. Pharmacokinetics of G-ZO Nps ligands and zinc acetate calculated with the SwissADME database.

COMPOUNDS	Rutin	Isoquercetin	Apigenin	Myricetin 3-O-galactoside	Zinc acetate
Gastrointestinal absorption	Low	Low	High	Low	Low
Bioavailability score	0.17		0.55	0.17	0.55
Blood–brain barrier permeation	No	No	No	No	No
P-glycoprotein substrate	Yes	No	No	No	Yes
Cytochrome P450 1A2 inhibitor	No	No	Yes	No	No
Cytochrome P450 2C19 inhibitor	No	No	No	No	No
Cytochrome P450 2C9 inhibitor	No	No	No	No	No
Cytochrome P450 2D6 inhibitor	No	No	Yes	No	No
Cytochrome P450 3A4 inhibitor	No	No	Yes	No	No

Table 9. Drug-likeness and medicinal chemistry characteristics of G-ZO Nps ligands and zinc acetate evaluated with the SwissADME database.

Compound	Drug-likeness rules					Medicinal chemistry			
	Lipinski	Ghose	Veber	Egan	Muegge	PAINS	Brenk	Lead likeness	Synthetic accessibility
Rutin	No; 3 violation	No	No	No	No	0 alert	0 alert	No; 1 violation	6.34
Isoquercetin	No; 2 violations	No	No	No	No	1 alert:	1 alert:	No	5.32
Apigenin	Yes: 0 violation	Yes	Yes	Yes	Yes	0 alert	0 alert	Yes	2.96
Myricetin 3-O-galactoside	No; 2 violation	No	No	No	No	1 alert	1 alert	No; 1 violation	5.36
Zinc acetate	Yes; 0 violation	No	Yes	Yes	No	0 alert	1 alert; heavy metals	No; 1 violation	1.00

Table 10. Summary of the docking scores of the five shortlisted ligands and zinc acetate across the three targets.

Ligand	1J46 (kcal/mol)	1T7R (kcal/mol)	3HDZ (kcal/mol)	Observation
Hesperidin	–7.0	–7.9	–12.2	Best on 3HDZ
Rutin	–7.5	–9.0	–11.5	Strongest on 1T7R
Apigenin	–6.6	–8.1	–9.8	Consistent across all
Isoquercetin	–6.9	–8.0	–9.8	Good overall
Myricetin 3-O-galactoside	–6.7	–7.7	–9.9	Strong docking
Zinc acetate (standard)	–1.0	–1.3	–1.3	Weak binding

Table 11. Summary of the key parameters used for the final selection of the three ligands.

Parameter	Hesperidin	Rutin	Apigenin	Isoquercetin	Myricetin 3-O-galactoside	Zinc acetate
Molecular Weight (g/mol)	~610	610	270	464	480	183
TPSA (Å²)	>230	234	90.9	210	230	80.26
GI Absorption	Low	Low	High	Low	Low	Low
Lipinski Violations	3	3	0	2	2	0
Bioavailability Score	0.17	0.17	0.55	0.17	0.17	0.55
Drug-likeness	Poor	Poor	Good	Moderate	Moderate	Poor (metal ion)

4.3. Results of the Receptor-ligand interactions between the docked ligands and proteins.

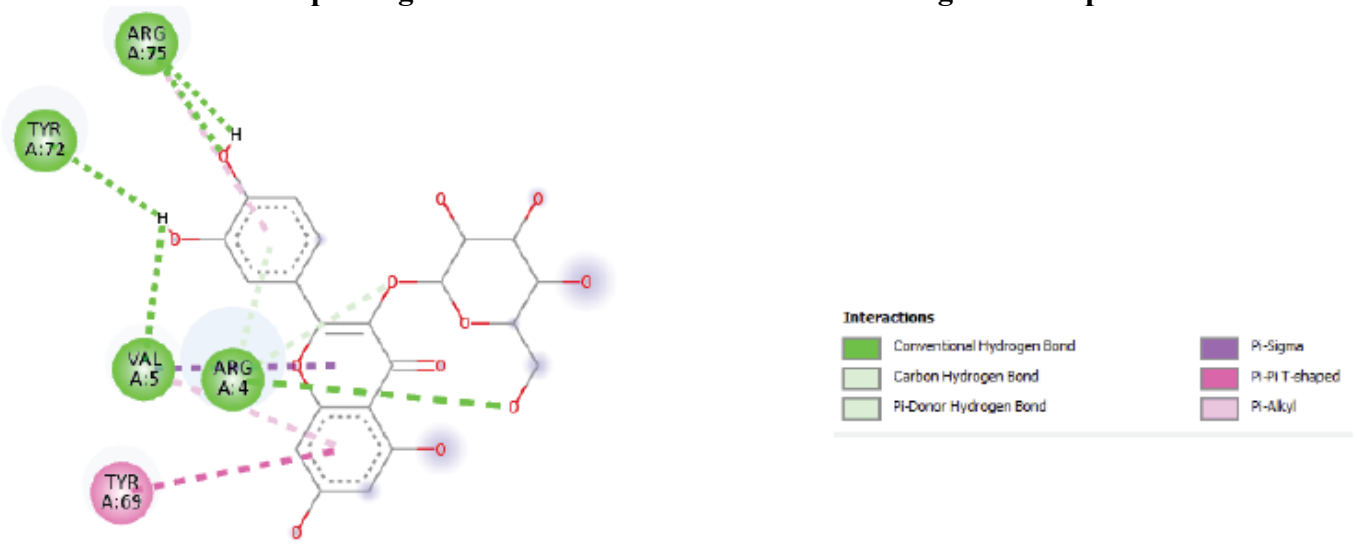

Figure 12 (a). Isoquercetin with 1j46.

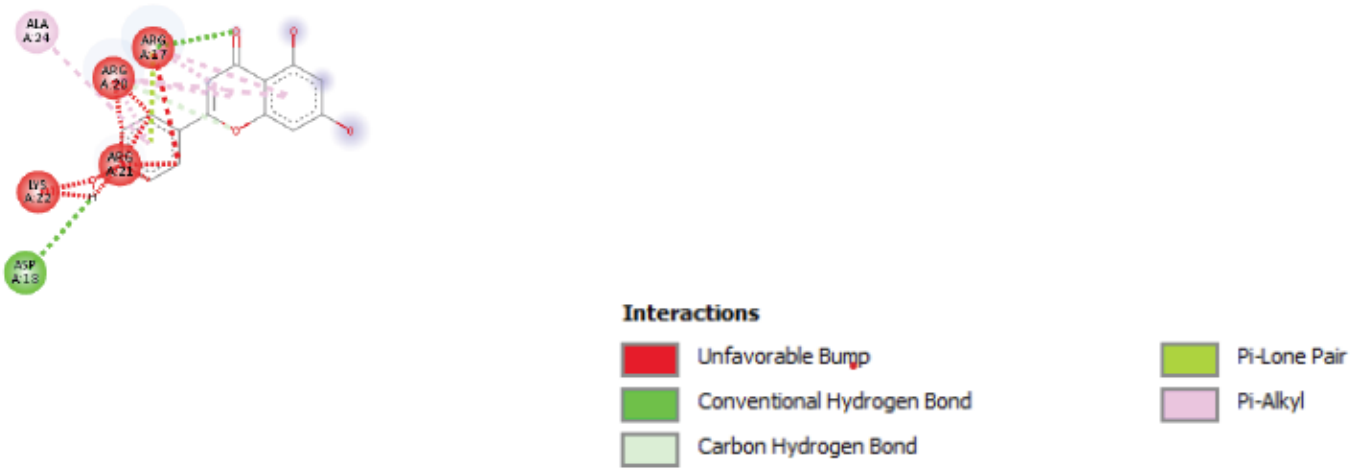

Figure 12 (b). Apigenin with 1j46.

Figure 12 (c). Myricetin-O-galactoside with 1j46.

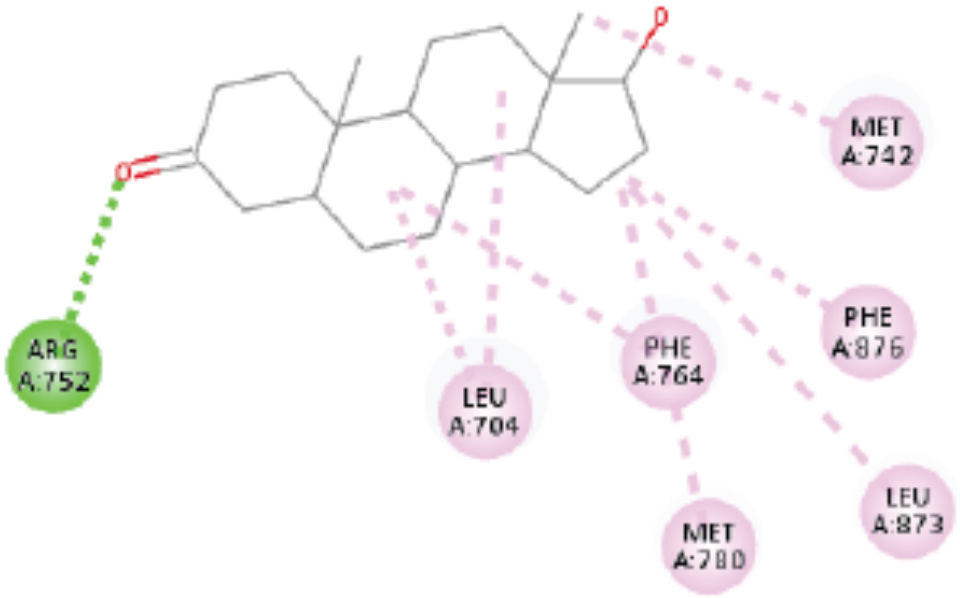

Figure 12 (d). Apigenin with 1t7r.

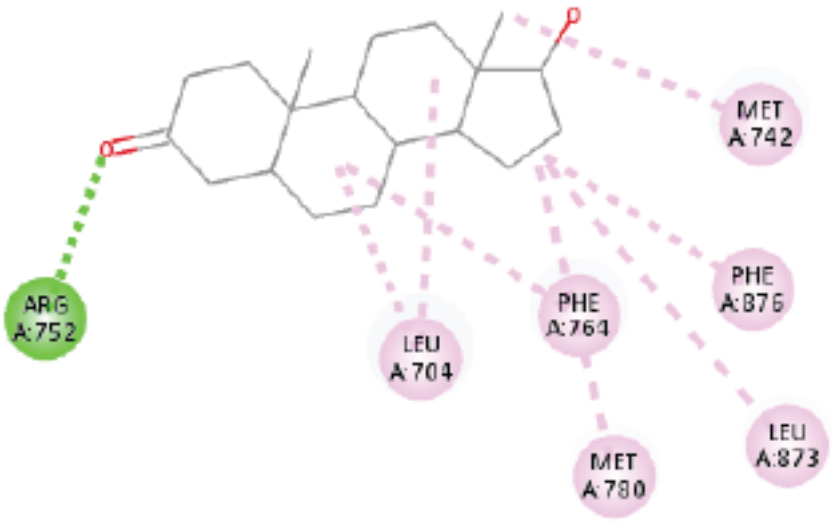

Figure 12 (e). Isoquercetin with 1t7r.

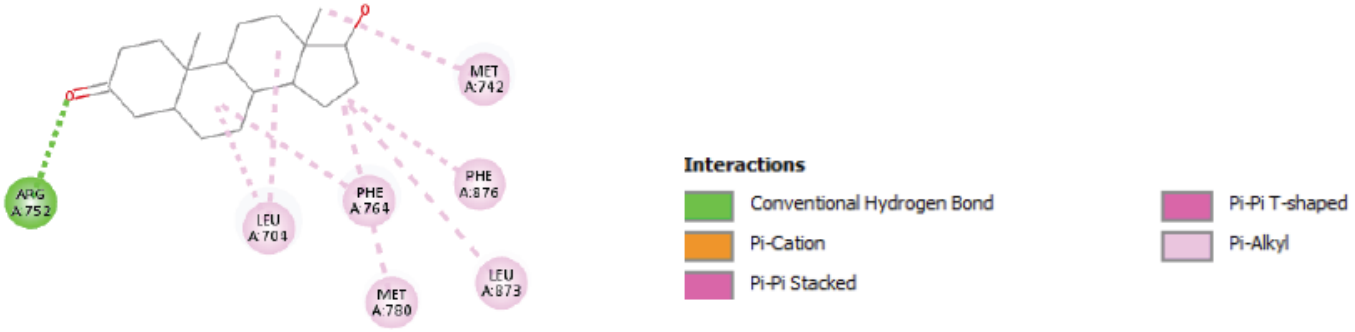

Figure 12 (f). myricetin-3-O-galactoside with 1t7r.

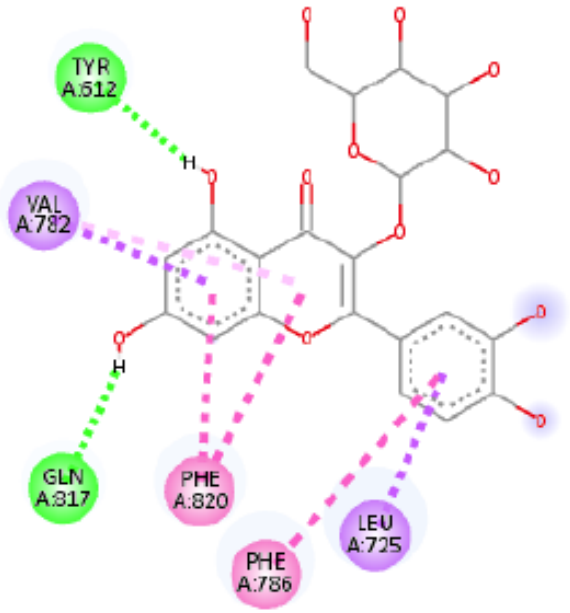

Figure 12 (g). isoquercetin with 3hdz.

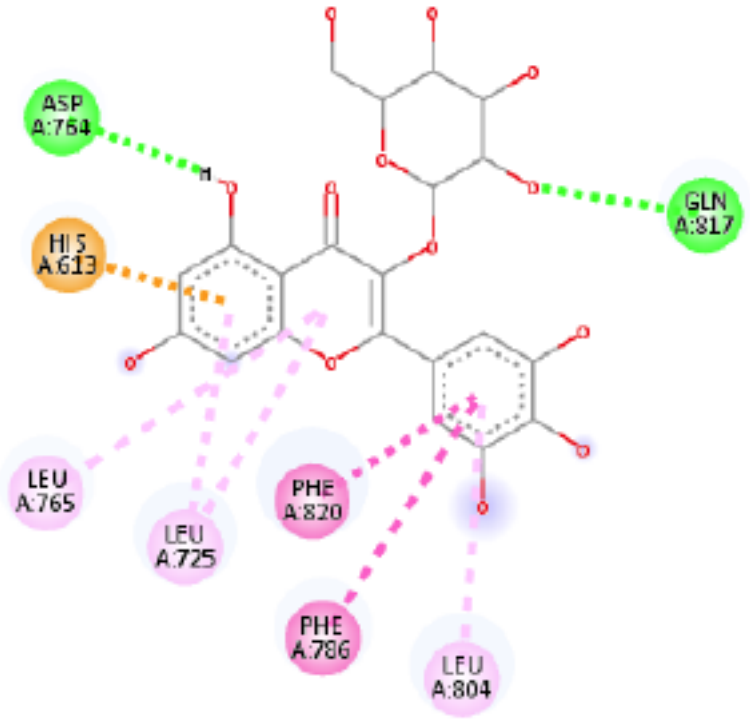

Figure 12 (h). myricetin-3-O-galactoside with 3hdz.

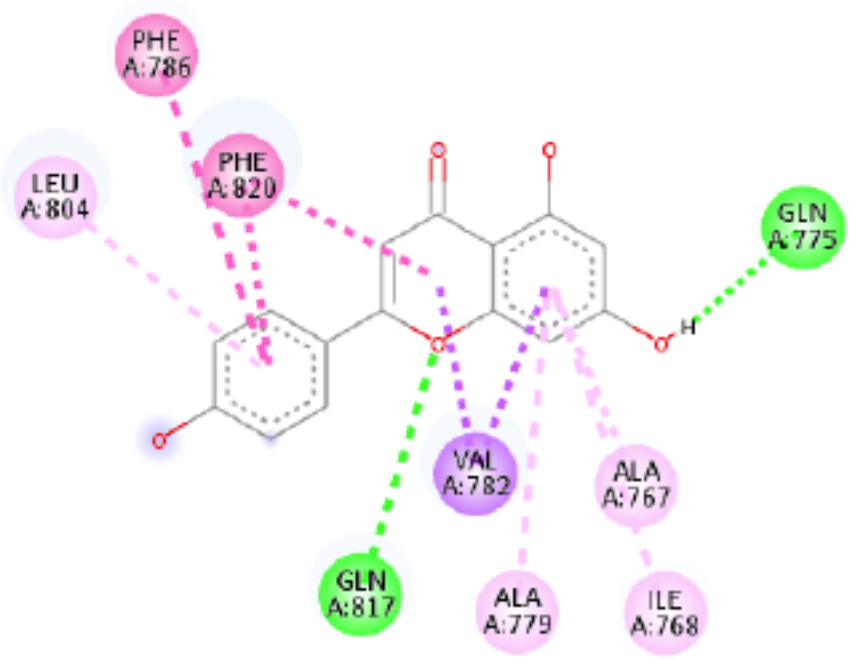

Figure 12 (i). Apigenin with 3hdz.

DISCUSSIONS

Lead exposure is widely recognized to induce oxidative stress, primarily by disrupting the balance between pro-oxidants and antioxidant defenses in cells (Abu-Khudir *et al.,* 2023). This imbalance adversely affects testicular function by damaging germ cells, impairing steroidogenesis, and altering the structural

integrity of seminiferous tubules (Haouas *et al.,* 2015). Ginger, rich in bioactive phytochemicals, and zinc, an essential trace element in spermatogenesis, both exhibit repro-protective effects (Bordbar *et al.,* 2013). In the present study, the protective effects of green-synthesized ginger–zinc oxide nanoparticles (G-ZO NPs) were evaluated against lead nitrate-induced testicular toxicity in Wistar rats, integrating biochemical, histological, and in silico evidence.

One of the earliest alterations observed was a significant elevation in NO levels in the $PbNO_3$ group, reflecting nitrosative stress commonly associated with lead toxicity. Excessive NO reacts with superoxide to generate peroxynitrite, a reactive oxidant that impairs lipid membranes, proteins, and DNA. Treatment with G-ZO NPs and ginger extract effectively reduced NO levels, consistent with reports that phytochemicals in ginger possess potent NO-scavenging activity (Abolaji *et al.,* 2017). This suggests that nanoparticle-based delivery not only enhances bioavailability but also strengthens radical-scavenging capacity beyond that observed with ginger or zinc alone.

Unexpectedly, MDA level, a standard index of lipid peroxidation, was not significantly elevated in the $PbNO_3$ group compared with controls. This finding contrasts with several reports that consistently demonstrate increased MDA following lead exposure in testicular tissue (Gharibshahi *et al.,* 2025). A plausible explanation is the compensatory activation of GPx, which detoxifies lipid hydroperoxides and could have limited MDA accumulation during the 28-day exposure period as was similarly reported by Abarikwu et al. (2016) in a three (3) weeks exposure window. In addition, the TBARS assay used for MDA measurement has known limitations in sensitivity and specificity, which may have masked subtle oxidative changes (Abeyrathne *et al.,* 2021). Previous studies have also shown that oxidative stress does not always manifest as elevated MDA, particularly in tissues such as the testes where antioxidant defenses like GPx are robust (García-Díaz *et al.,* 2015). In an older study, Unlucerc et al. (2000) also reported a diabetes-induced increase in testicular GPx activities without concomitant rise in MDA levels, indicating strong enzymatic defense against oxidative stress in the testis. Interestingly, while zinc nanoparticles have been reported to reduce MDA at lower doses in doxorubicin- and levofloxacin-induced toxicity (El-Maddawy *et al.,* 2019**;** Zaki *et al.,* 2024), the lack of a significant reduction in our treated groups may reflect the already elevated baseline antioxidant defense in the lead group, leaving little room for further detectable improvement.

This interpretation is supported by the observation that GPx activity was significantly elevated in the $PbNO_3$ group compared to both control and treated groups. GPx is central to the detoxification of hydrogen peroxide and lipid hydroperoxides, using reduced glutathione as a cofactor Jomova *et al.,* 2024). Its marked elevation here suggests a compensatory response to oxidative stress, as reported in other models of heavy-metal toxicity (Sobeková *et al.,* 2009; Bas, and Kalender, 2016). Interestingly, the return of GPx activity toward baseline in G-ZO NP-treated rats implies that exogenous antioxidants reduced oxidative burden, thereby lowering the need for heightened endogenous enzyme activity. This contrasts with earlier studies where lead exposure was shown to suppress GPx activity (Sudjarwo *et al.,* 2017; Amer *et al.,* 2025), suggesting that the magnitude and duration of exposure, as well as tissue-specific antioxidant capacity, can determine the direction of GPx modulation.

Parallel to this, SOD and CAT activities were significantly enhanced in treated groups. SOD converts superoxide radicals into hydrogen peroxide, while CAT rapidly decomposes hydrogen peroxide into water and oxygen, thereby limiting hydroxyl radical formation (Niki, 2018). The marked elevation of SOD in the G-ZO NP group compared to $PbNO_3$ alone underscores the efficiency of nanoparticle-mediated delivery in sustaining antioxidant activity within testicular tissue. Similarly, CAT activity was significantly elevated in all treated groups, which aligns with previous reports that zinc nanoparticles and plant phytochemicals restore CAT under oxidative stress conditions (Sun *et al.,* 2023; Shkal *et al.,* 2020). Together, these enzymatic responses highlight the reinforcement of primary antioxidant defenses against lead-induced oxidative damage.

Although changes in reduced glutathione were modest and not statistically significant, the slight elevation observed in treatment groups compared to $PbNO_3$ suggests partial restoration of redox balance. Given that GSH is a vital intracellular thiol responsible for free radical scavenging and GPx activity (Averill-Bates, 2023; Chai and Mieyal, 2023), this trend reflects the overall protective role of G-ZO NPs, even if

not dramatic in magnitude. It is possible that the administered antioxidants preferentially boosted enzymatic pathways rather than directly increasing GSH stores, explaining the subtle effect observed.

These biochemical findings were corroborated by histological evaluation. Testes from $PbNO_3$-exposed rats exhibited expanded lumens and interstitial cell hypertrophy, characteristic of impaired spermatogenesis, whereas those from the G-ZO NP-treated group displayed largely preserved seminiferous tubules with intact germinal architecture. Ginger and zinc acetate provided partial protection, consistent with their less pronounced biochemical effects. Importantly, no necrosis or fibrosis was observed across groups, indicating that at the given dose and duration, lead caused functional disruption without overt cytotoxicity, thus suggesting that short-term/sub-acute lead exposure induces oxidative imbalance which may precede or occur without gross histopathological lesions depending on dose, tissue, and exposure duration (Offor *et al.,* 2019; Vukelić *et al.,* 2023).

Finally, in silico docking analyses provided mechanistic support for the protective effects observed *in vivo*. Flavonoids identified in G-ZO NPs, particularly apigenin, isoquercetin, and myricetin-3-O-galactoside, demonstrated strong binding affinities to the androgen receptor, PDE-5, and SRY protein. These interactions suggest regulatory roles in androgen signaling, nitric oxide pathways, and spermatogenic transcription, which collectively underpin reproductive protection. Apigenin, in particular, exhibited favorable pharmacokinetics, including high gastrointestinal absorption and no Lipinski violations, reinforcing its translational relevance. By contrast, zinc acetate displayed weak receptor interactions, consistent with its limited protective capacity *in vivo*. The strong ligand–protein interactions of nanoparticle-encapsulated flavonoids therefore explain the superior performance of G-ZO NPs compared to ginger extract or zinc acetate, aligning with earlier reports on flavonoid and zinc oxide nanoparticles mediated reproductive protection (D'Arrigo *et al.,* 2021; Attia *et al.,* 2021).

Taken together, these findings demonstrate that G-ZO NPs mitigate lead-induced testicular toxicity through a multifaceted mechanism involving modulation of oxidative stress, reinforcement of enzymatic defenses, and preservation of testicular histoarchitecture. The integration of *in vivo* and in silico evidence highlights the potential of nanoparticle-based phytomedicine as a promising strategy for reproductive protection, while also offering novel insights into the compensatory dynamics of antioxidant systems under heavy-metal stress.

CONCLUSION

This research elucidated the biochemical and molecular efficacy of green-synthesized ginger-zinc oxide nanoparticles (G-ZO NPs) in ameliorating lead-induced testicular oxidative stress and dysfunction. The successful fabrication of G-ZO NPs, characterized by UV-Vis spectroscopy, FTIR, SEM-EDX, and HPLC, confirmed the encapsulation of bioactive flavonoids—such as apigenin, isoquercetin, and naringenin—within a nanoscale zinc oxide matrix, enhancing their bioavailability and redox activity. Biochemical assays demonstrated that G-ZO NP administration significantly modulated oxidative stress markers by attenuating nitric oxide and malondialdehyde levels, while restoring the activities of endogenous antioxidant enzymes including superoxide dismutase (SOD), catalase (CAT), glutathione peroxidase (GPx), and glutathione (GSH). These outcomes suggest effective scavenging of reactive oxygen and nitrogen species (ROS/RNS) and reinforcement of the testicular antioxidant defense system.

Histopathological analysis further confirmed the cytoprotective potential of G-ZO NPs, as evidenced by the preservation of seminiferous tubule architecture and reduced testicular degeneration relative to untreated toxicant-exposed rats. Molecular docking studies substantiated these findings by revealing strong ligand–receptor interactions between key phytoconstituents and target proteins involved in androgenic signaling and nitric oxide regulation (AR, PDE-5, and SRY). In summary, this study presents compelling evidence that G-ZO NPs potentiate biochemical resilience and structural integrity in testicular tissue under toxic metal-induced stress. The synergistic integration of phytotherapy and nanotechnology thus offers a promising avenue for the development of targeted antioxidative interventions in reproductive toxicology.

AUTHORS' CONTRIBUTIONS

The author confirms sole responsibility for the following: study conception and design, data collection, analysis and interpretation of results, and manuscript preparation.

CONSENT FOR PUBLICATION

Not applicable.

FUNDING

None.

CONFLICT OF INTEREST

The author confirms that this article's content has no conflict of interest.

ACKNOWLEDGEMENTS

The Authors wish to acknowledge the managements of Osun State University, Osogbo and Adeleke University Ede, for making necessary technical facilities available to enhance the success of this research work.

REFERENCES

Abarikwu, S. O., Duru, Q. C., Chinonso, O. V., & Njoku, R. C. (2016). Antioxidant enzymes activity, lipid peroxidation, oxidative damage in the testis and epididymis, and steroidogenesis in rats after co-exposure to atrazine and ethanol. *Andrologia, 48*(5), 548–557. https://doi.org/10.1111/and.12478

Abeyrathne, E. D. N. S., Nam, K., & Ahn, D. U. (2021). Analytical methods for lipid oxidation and antioxidant capacity in food systems. *Antioxidants, 10*(10), 1587. https://doi.org/10.3390/antiox10101587

Abolaji, A. O., Ojo, M., Afolabi, T. T., Arowoogun, M. D., Nwawolor, D., & Farombi, E. O. (2017). Protective properties of 6-gingerol-rich fraction from *Zingiber officinale* (ginger) on chlorpyrifos-induced oxidative damage and inflammation in the brain, ovary and uterus of rats. *Chemico-Biological Interactions, 270*, 15–23. https://doi.org/10.1016/j.cbi.2017.03.017

Abu-Khudir, R., Almutairi, H. H., Abd El-Rahman, S. S., & El-Said, K. S. (2023). The palliative and antioxidant effects of hesperidin against lead-acetate-induced testicular injury in male Wistar rats. *Biomedicines, 11*(9), 2390. https://doi.org/10.3390/biomedicines11092390

Aebi, H. (1984). Catalase *in vitro*. In *Methods in Enzymology* (Vol. 105, pp. 121–126). https://doi.org/10.1016/S0076-6879(84)05016-3

Al-Darwesh, M., & Ibrahim, S. (2024). A review on plant extract mediated green synthesis of zinc oxide nanoparticles and their biomedical applications. *Results in Chemistry, 7,* 101368. https://doi.org/10.1016/j.rechem.2024.101368

Alhaddad, R., Abualsoud, B. M., Al-Deeb, I., & Nsairat, H. (2024). Green synthesized *Zingiber officinale*–ZnO nanoparticles: Anticancer efficacy against 3D breast cancer model. *Future Science OA, 10*(1), Article 2419806. https://doi.org/10.1080/20565623.2024.2419806

Al-Suwayyid, L. S. A., Janakiraman, A. K., Thiagarajah, S., Gunasekaran, B., Khanna, K., Kumar, A., Mohamed, J. M. M., & Wong, L. S. (2023). Green synthesis of ginger-encapsulated zinc oxide nanoparticles: Unveiling their characterization and selective cytotoxicity on MDA-MB 231 breast cancer cells. *Journal of Advanced Pharmaceutical Technology & Research, 14*(4), 325–331. https://doi.org/10.4103/JAPTR.JAPTR_313_23

Amer, N., Ibrahim, N., Ibrahim, B., & Agaga, R. (2025). Histological and biochemical analysis of the possible protective effects of luteolin on testicular injury caused by lead acetate in adult male albino rats. *Mansoura Journal of Forensic Medicine and Clinical Toxicology, 33*(1), 13–32. https://doi.org/10.21608/mjfmct.2024.309523.1084

Attia, G. H., Moemen, Y. S., Youns, M., Ibrahim, A. M., Abdou, R., & El Raey, M. A. (2021). Antiviral zinc oxide nanoparticles mediated by hesperidin and in silico comparison study between antiviral phenolics as anti-SARS-CoV-2. *Colloids and Surfaces B: Biointerfaces, 203*, 111724. https://doi.org/10.1016/j.colsurfb.2021.111724

Averill-Bates, D. A. (2023). The antioxidant glutathione. *Vitamins and Hormones, 121*, 109–141. https://doi.org/10.1016/bs.vh.2022.09.002

Bas, H., & Kalender, S. (2016). Antioxidant status, lipid peroxidation and testis-histoarchitecture induced by lead nitrate and mercury chloride in male rats. *Brazilian Archives of Biology and Technology, 59*, e16160151. https://doi.org/10.1590/1678-4324-2016160151

Besong, E. E., Ashonibare, P. J., Obembe, O. O., Folawiyo, M. A., Adeyemi, D. H., Hamed, M. A., Akhigbe, T. M., & Akhigbe, R. E. (2023). Zinc protects against lead-induced testicular damage *via* modulation of steroidogenic and xanthine oxidase/uric acid/caspase-3-mediated apoptotic signaling in male Wistar rats. *The Aging Male, 26*(1), 2224428. https://doi.org/10.1080/13685538.2023.2224428

Bordbar, H., Esmaeilpour, T., Dehghani, F., & Panjehshahin, M. R. (2013). Stereological study of the effect of ginger's alcoholic extract on the testis in busulfan-induced infertility in rats. *Iranian Journal of Reproductive Medicine, 11*(6), 467–472. https://www.ncbi.nlm.nih.gov/pmc/articles/PMC3941314/

Chai, Y. C., & Mieyal, J. J. (2023). Glutathione and glutaredoxin—Key players in cellular redox homeostasis and signaling. *Antioxidants, 12*(8), 1553. https://doi.org/10.3390/antiox12081553

D'Arrigo, G., Gianquinto, E., Rossetti, G., Cruciani, G., Lorenzetti, S., & Spyrakis, F. (2021). Binding of androgen- and estrogen-like flavonoids to their cognate (non)nuclear receptors: A comparison by computational prediction. *Molecules, 26*(6), 1613. https://doi.org/10.3390/molecules26061613

Ellman, G. L. (1959). Tissue sulfhydryl groups. *Archives of Biochemistry and Biophysics, 82*(1), 70–77. https://doi.org/10.1016/0003-9861(59)90090-6

El-Maddawy, Z. K., & Abd El Naby, W. S. H. (2019). Protective effects of zinc oxide nanoparticles against doxorubicin induced testicular toxicity and DNA damage in male rats. *Toxicology Research (Cambridge), 8*(5), 654–662. https://doi.org/10.1039/c9tx00052f

Funmilola, A. S., & Ayodeji, A. D. (2025). Raw and boiled ginger (*Zingiber officinale* Roscoe) inclusive diet improves fertility parameters in high cholesterol diet-induced obese rats. *BMC Complementary Medicine and Therapies, 25*(1), 209. https://doi.org/10.1186/s12906-025-04948-1

García-Díaz, E. C., Gómez-Quiroz, L. E., Arenas-Ríos, E., Aragón-Martínez, A., Ibarra-Arias, J. A., & Retana-Márquez, M. S. I. (2015). Oxidative status in testis and epididymal sperm parameters after acute and chronic stress by cold-water immersion in the adult rat. *Systemic Biology of Reproduction and Medicine, 61*(3), 150–160. https://doi.org/10.3109/19396368.2015.1008071

Gharibshahi, N., Gazwi, H. S. S., Khosravi, M., Khosravi-Farsani, S., Khadivi, F., & Zarei, M. H. (2025). Galbanic acid alleviates lead acetate-induced reproductive toxicity in prepubertal male Wistar rats. *Scientific Reports, 15*, 22508. https://doi.org/10.1038/s41598-025-06661-y

Gholami-Ahangaran, M., Karimi-Dehkordi, M., Akbari Javar, A., Haj Salehi, M., & Ostadpoor, M. (2021). A systematic review on the effect of ginger (*Zingiber officinale*) on improvement of biological and fertility indices of sperm in laboratory animals, poultry, and humans. *Veterinary Medicine and Science, 7*(5), 1959–1969. https://doi.org/10.1002/vms3.538

Haouas, Z., Zidi, I., Sallem, A., Bhouri, R., Ajina, T., Zaouali, M., & Mehdi, M. (2015). Reproductive toxicity of lead acetate in adult male rats: Histopathological and cytotoxic studies. *Journal of Cytology & Histology, 6*, 293. https://doi.org/10.4172/2157-7099.1000293

Jaishi, D. R., Ojha, I., Bhattarai, G., Baraili, R., Pathak, I., Ojha, D. R., Shrestha, D. K., & Sharma, K. R. (2024). Plant-mediated synthesis of zinc oxide (ZnO) nanoparticles using *Alnus nepalensis* D. Don for biological applications. *Heliyon, 10*(20), e39255. https://doi.org/10.1016/j.heliyon.2024.e39255

Jomova, K., Alomar, S. Y., Alwasel, S. H., Nepovimova, E., Kuca, K., & Valko, M. (2024). Several lines of antioxidant defense against oxidative stress: Antioxidant enzymes, nanomaterials with multiple enzyme-mimicking activities, and low-molecular-weight antioxidants. *Archives of Toxicology, 98*, 1323–1367. https://doi.org/10.1007/s00204-024-03696-4

Kumar, A., Kumar, A., Chaturvedi, A. K., Shabnam, A. A., Subrahmanyam, G., Mondal, R., Gupta, D. K., Malyan, S. K., Kumar, S. S., Khan, S. A., & Yadav, K. K. (2020). Lead toxicity: Health hazards, influence on food chain, and sustainable remediation approaches. *International Journal of Environmental Research and Public Health, 17*(7), 2179. https://doi.org/10.3390/ijerph17072179

Maher, A. M., Elsanosy, G. A., Ghareeb, D. A., Elblehi, S. S., & Saleh, S. R. (2025). 10-Hydroxy decanoic acid and zinc oxide nanoparticles retrieve Nrf2/HO-1 and caspase-3/Bax/Bcl-2 signaling in lead-induced testicular toxicity. *Biological Trace Element Research, 203*(5), 2728–2751. https://doi.org/10.1007/s12011-024-04374-3

Misra, H. P., & Fridovich, I. (1972). The role of superoxide anion in the autooxidation of epinephrine and a simple assay for superoxide dismutase. *Journal of Biological Chemistry, 247*(10), 3170–3175.

Mutukwa, D., Taziwa, R. T., & Khotseng, L. (2024). A review of plant-mediated ZnO nanoparticles for photodegradation and antibacterial applications. *Nanomaterials, 14*(14), 1182. https://doi.org/10.3390/nano14141182

Niki, E. (2018). Oxidant-specific biomarkers of oxidative stress: Association with atherosclerosis and implication for antioxidant effects. *Free Radical Biology and Medicine, 120*, 425–440. https://doi.org/10.1016/j.freeradbiomed.2018.04.001

Offor, S. J., Mbagwu, H. O., & Orisakwe, O. E. (2019). Improvement of lead acetate-induced testicular injury and sperm quality deterioration by *Solanum anomalum* Thonn. ex. Schumach fruit extracts in albino rats. *Journal of Family & Reproductive Health, 13*(2), 98–108. https://www.ncbi.nlm.nih.gov/pmc/articles/PMC6969887/

Rotruck, J. T., Pope, A. L., Ganther, H. E., Swanson, A. B., Hafeman, D. G., & Hoekstra, W. (1973). Selenium: Biochemical role as a component of glutathione peroxidase. *Science, 179*(4073), 588–590. https://doi.org/10.1126/science.179.4073.588

Shkal, K. E. M., Azab, A. E., Attia, A. M., El-Banna, S. G., & Yahya, R. A. M. (2020). Zinc oxide nanoparticles attenuate the oxidative damage and disturbance in antioxidant defense system induced by cyclophosphamide in male albino rats. *Insights in Biology and Medicine, 4*, 001–008.

Sobeková, A., Holovská, K., Lenártová, V., Legáth, J., & Javorskỳ, P. (2009). The alteration of glutathione peroxidase activity in rat organs after lead exposure. *Acta Physiologica Hungarica, 96*(1), 37–44. https://doi.org/10.1556/APhysiol.96.2009.1.4

Sudjarwo, S. A., Sudjarwo, G. W., & Koerniasari. (2017). Protective effect of curcumin on lead acetate-induced testicular toxicity in Wistar rats. *Research in Pharmaceutical Sciences, 12*(5), 381–390. https://doi.org/10.4103/1735-5362.213983

Sun, L., Wang, R., Ju, Q., Xing, M., Li, R., Li, W., Li, W., Wang, W., Deng, Y., & Xu, J. (2023). Mitigation mechanism of zinc oxide nanoparticles on cadmium toxicity in tomato. *Frontiers in Plant Science, 14*, 1162372. https://doi.org/10.3389/fpls.2023.1162372

Trenkenschuh, E., & Friess, W. (2021). Freeze-drying of nanoparticles: How to overcome colloidal instability by formulation and process optimization. *European Journal of Pharmaceutics and Biopharmaceutics, 165,* 345–360. https://doi.org/10.1016/j.ejpb.2021.05.024

Tuncer, Ş. Ç., Akarsu, S. A., Küçükler, S., Gür, C., & Kandemir, F. M. (2023). Effects of sinapic acid on lead acetate-induced oxidative stress, apoptosis, and inflammation in testicular tissue. *Environmental Toxicology, 38*(11), 2656–2667. https://doi.org/10.1002/tox.23900

Unlüçerçi, Y., Bekpinar, S., & Koçak, H. (2000). Testis glutathione peroxidase and phospholipid hydroperoxide glutathione peroxidase activities in aminoguanidine-treated diabetic rats. *Archives of Biochemistry and Biophysics, 379*(2), 217–220. https://doi.org/10.1006/abbi.2000.1876

Unuofin, J. O., Masuku, N. P., Paimo, O. K., & Lebelo, S. L. (2021). Ginger from farmyard to town: Nutritional and pharmacological applications. *Frontiers in Pharmacology, 12,* 779352. https://doi.org/10.3389/fphar.2021.779352

Vukelić, D., Djordjevic, A. B., Anđelković, M., Antonijević Miljaković, E., Baralić, K., Živančević, K., Bulat, P., Radovanović, J., Đukić-Ćosić, D., Antonijević, B., & Bulat, Z. (2023). Subacute exposure to low Pb doses promotes oxidative stress in the kidneys and copper disturbances in the liver of male rats. *Toxics, 11*(3), 256. https://doi.org/10.3390/toxics11030256

Zaki, N. F., Orabi, S. H., Abdel-Bar, H. M., Elbaz, H. T., Korany, R. M. S., Ismail, A. K., Daoush, W. M., Abduljabbar, M. H., Alosaimi, M. E., Alnemari, R. M., Mahboub, H. H., & Ahmed, M. M. (2024). Zinc oxide resveratrol nanoparticles ameliorate testicular dysfunction due to levofloxacin-induced oxidative stress in rats. *Scientific Reports, 14*, 2752. https://doi.org/10.1038/s41598-024-52830-w

Zheng, Y., Zhang, Q., Jing, L., Fei, Y., & Zhao, H. (2023). The effects of chronic lead exposure on testicular development of Japanese quail (*Coturnix japonica*): Histopathological damages, oxidative stress, steroidogenesis disturbance, and hypothalamus–pituitary–testis axis disruption. *Biological Trace Element Research, 201*(7), 3446–3460. https://doi.org/10.1007/s12011-022-03436-8